Intermetallic Compounds Formation in Dissimilar Friction Stir Welding of Mg/Cu Alloys

Xue Li[1] · Qingzhen Zhao[1] · Hao Su[1] · Ji Chen[1] · Chuansong Wu[1]

Abstract

Joining dissimilar Mg/Cu alloys was still an intractable problem because of the excessive intermetallic compounds (IMCs) and poor mechanical properties using conventional welding methods. In the present study, friction stir welding was employed for the butt joining of dissimilar AZ31B Mg-alloy and T2 pure Cu plates. Defect-free Mg/Cu joints were obtained with Mg-RS and Cu-AS configuration, at a welding speed of 50 mm/min and tool rotating speeds of 325 r/min, 625 r/min and 925 r/min. At the joining interface, both Mg_2Cu and $MgCu_2$ IMC phases were observed, with a clear, uniform and continuous IMCs layer composed of two sub-layers, layer-A of $Mg + Mg_2Cu$ and layer-B of $Mg_2Cu + MgCu_2$. The maximum ultimate tensile strength of the Mg/Cu friction stir welding joint reached 130 MPa at 925 r/min due to enhanced mechanical interlocking between Mg and Cu, as well as sufficient metallurgical bonding at the joining interface with an IMCs layer thickness in the range of 1.0–2.0 μm.

Keywords Friction stir welding · Magnesium · Copper · Intermetallic compounds · Mechanical properties

1 Introduction

Nowadays, magnesium (Mg), copper (Cu) and their alloys have received great attention in the applications of aerospace, automobile, lightweight manufacturing and other industrial fields because of their excellent mechanical properties [1–3]. Joining dissimilar Mg/Cu alloys is particularly important since it will promote the design flexibility of the dissimilar metals inside a single structural component [4]. Mg-Cu bimetals are widely used in the electronic and electrical industries, electrical appliances, machinery and automotive industries, and their research and application have expanded beyond navigation and military fields to include high-value civil products like automobiles, computers, and communication equipment. However, due to the large differences in the physical and mechanical properties between Mg and Cu, it is still a big challenge to obtain high-quality dissimilar Mg/Cu joints with proper formation of intermetallic compounds (IMCs) between Mg and Cu, which prevents the application of Mg-Cu hybrid structure in the industry [5–7].

Some attempts at dissimilar Mg/Cu joining have been carried out by employing various welding methods. Zhao et al. [8] conducted ultrasonic welding between AZ31B Mg alloy and pure Cu and analyzed the microstructure and mechanical properties of the dissimilar joints. The Mg plate underwent significant deformation with the welding temperature reaching 550 °C, but the maximum joining strength was only 3798 N. Shan et al. [9] investigated the feasibility of resistance spot welding to achieve successful joining of dissimilar Mg/Cu alloys with defect-free weld nugget, but the maximum tensile shear load of the joint was less than 2626 N with poor ductility. Mahendran et al. [10] optimized the process parameters in diffusion bonding of dissimilar Mg/Cu alloys, and the maximum bonding strength reached 81 MPa with bonding temperature, pressure and time of 450 °C, 12 MPa and 30 min, respectively. Liu et al. [11] obtained dissimilar Mg/Cu lap joining by tungsten inert gas welding with Fe as an interlayer to implement re-melt deposit welding of Cu/Fe and brazing of Fe/Mg, without

✉ Hao Su
   suh@email.sdu.edu.cn

✉ Ji Chen
   chenji@sdu.edu.cn

1   MOE Key Lab for Liquid-Solid Structure Evolution
    and Materials Processing, Institute of Materials Joining,
    Shandong University, Jinan 250061, China

the formation of intermetallic compounds between Cu and Mg. However, although the above-mentioned methods are capable of joining dissimilar Mg/Cu, the joining strength is inadequate for industrial application requirements.

As a solid-state welding technique, friction stir welding (FSW) has the advantages of no cracks, small deformation and well-performed joint strength compared to traditional fusion welding. Compared to conventional diffusion welding, ultrasonic welding and TIG welding, an extra mechanical stirring effect is employed on the base metals, which is conducive to improving the mechanical interlocking degree of the dissimilar joint, thus increasing the final tensile strength [12]. FSW has great potential in connecting materials with different mechanical and chemical properties, including not only metals such as lightweight metals, like Al and Mg, as well as some of the dissimilar alloys [13–23] but also metal and nonmetal such as polymer [24, 25]. During the past decades, some innovative techniques in FSW have also sprung out, such as friction stir remanufacturing (FSR), friction stir double-riveting welding (FSDRW) and so on [24, 26]. Because of the relatively lower heat input and more intense plastic deformation during FSW, the IMCs of the dissimilar joints can be controlled and the joint strengths can be improved. However, few results about FSW of dissimilar Mg/Cu alloys have been reported so far. In this study, dissimilar alloys of AZ31B Mg and T2 pure Cu were butt welded by FSW, and the microstructure and mechanical properties of Mg/Cu FSW joints were analyzed. Besides, the distribution and formation of IMCs at the joining interface were discussed to further understand the joining mechanisms of the Mg/Cu FSW joints.

2 Experimental

In the experiments, plates of AZ31B Mg and T2 pure Cu with thickness of 3 mm were welded in butt joint configurations. During the welding process, Mg and Cu plates were placed at the retreating side (RS) and the advancing side (AS), respectively, on the backing plate, as schematically shown in Fig. 1a. The tool was made of H13 tool steel, and was composed of a concave shoulder and a right-hand threaded pin to produce sufficient heat generation and material flow [27]. The shoulder was with a diameter of 20 mm, the pin was with length of 2.80 mm, and the root and tip diameters of 4.2 mm and 3.2 mm, respectively, as shown in Fig. 1b. The tool rotating speeds were 325 r/min. 625 r/min and 925 r/min, while the welding speed was kept constant at 50 mm/min. Besides, the tool tilt angle was 1.5°, the plunging depth of the shoulder into the top surface of the plate was 0.1 mm, and no tool offset was considered. After welding, the metallographic samples and tensile specimens were cut by an electrical discharge wire cutting machine,
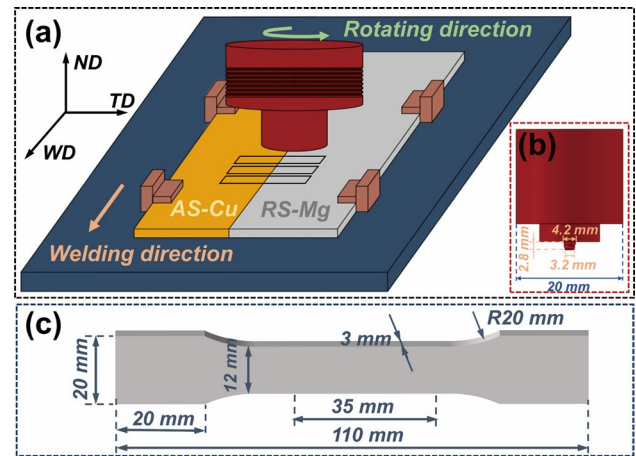
Fig. 1 Details of the experiment: **a** a schematic figure of Mg/Cu dissimilar FSW system, **b** dimensions of the tool, **c** specimens for tensile tests

and the specific size of the tensile specimen is shown in Fig. 1c. Then, the micrographs of the Mg/Cu FSW joints were taken by Zeiss Daheng Invasion USB camera microscope, and the IMCs at the joining interface were characterized by a JEOL JSM-7800F field emission scanning electron microscope (SEM), equipped with energy dispersive X-ray spectrometer (EDS, Oxford Instruments, XMax 80). Tensile tests were performed on a CMT-50 universal electronic tensile testing machine at room temperature and the tensile rate was set at 1 mm/min. Then, the fracture morphologies were analyzed to investigate the fracture behavior of the Mg/Cu FSW joints.

3 Results and Discussion

3.1 Macrostructure

Since it is well-known that mechanical interlocking and metallurgical bonding are two primary factors determining the joining strength in dissimilar FSW [28, 29], the macrostructure at the cross-section of the Mg/Cu joints with three tool rotating speeds is first analyzed, as depicted in Fig. 2. In this figure, the white dotted lines indicate the trace of the tool during the welding process. It is shown that defect-free Mg/Cu FSW joints are obtained by all three tool rotating speeds, and the dissimilar materials mix well with each other. The joining interface of the Mg/Cu joints is irregularly distributed and its total length exhibits an increasing trend with increasing tool rotating speeds. In the upper region of the joint with 325 r/min, Mg at the RS is squeezed into Cu at the AS, as shown in Fig. 2a. With increasing tool rotating speed to 625 r/min and 925 r/min, a long Cu piece at the AS is inserted into Mg at the RS, as shown in Fig. 2b and c,
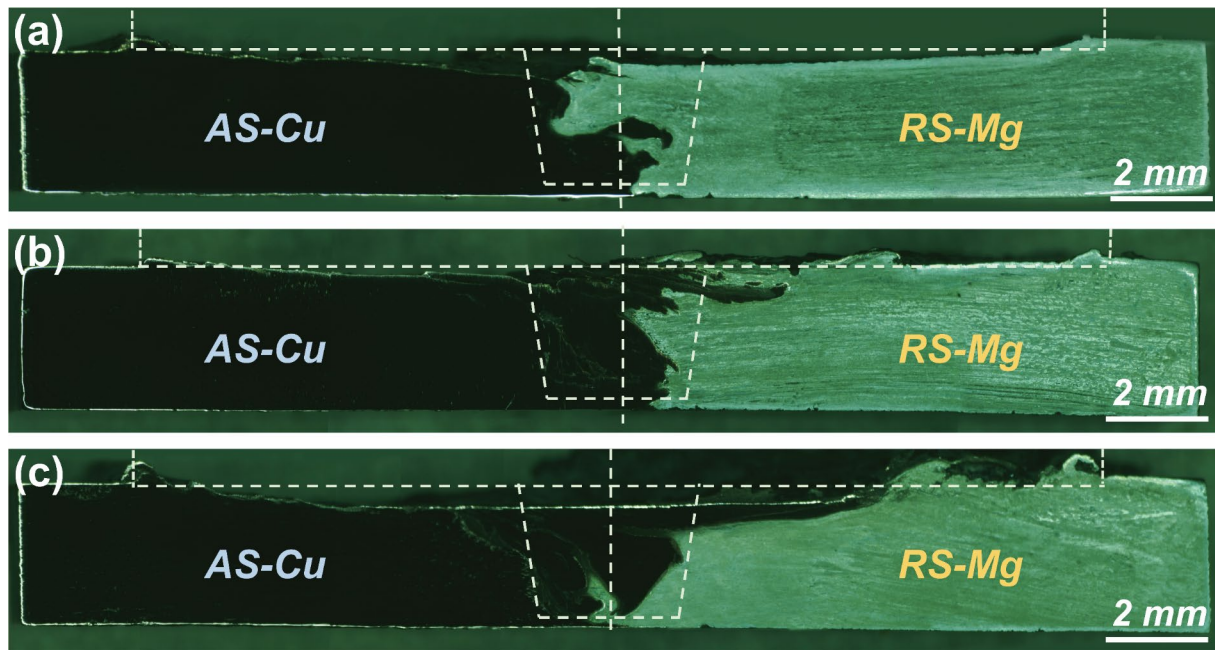
Fig. 2 Macroscopic observations of the Mg/Cu FSW joints with three tool rotating speeds: **a** 325 r/min, **b** 625 r/min, **c** 925 r/min

respectively. There is no doubt that the extension of the joining interface increases the contact area between Cu and Mg, which is beneficial for the weld quality. In the lower region, the intermixing between the dissimilar materials is also more distinct with 925 r/min compared with other tool rotating speeds. This phenomenon can be attributed to the stronger material flow caused by the tool with a threaded pin at a relatively higher tool rotating speed. Thus, the mechanical interlocking at the Mg/Cu joining interface can be improved.

3.2 Microstructure and IMCs

Figure 3 shows the SEM with the corresponding EDS mapping images at the Mg/Cu joining interface from the middle parts of the dissimilar FSW joints. The middle part is selected based on the consideration that the microstructure in this region is influenced by both the shoulder and the pin comparing that in the upper and the lower regions of the Mg/Cu joints. It can be seen that the interface is relatively blurry at tool rotating speeds of both 325 r/min and 625 r/min, which indicates that the interfacial reaction layer is restricted within a narrow limit of less than 0.5 μm. For a higher tool rotating speed of 925 r/min, the mutual diffusion between Mg and Cu at the interface is more evident and layered structures with a thickness of about 2.0 μm can be observed, as shown in Fig. 3i–l. The interfacial structures can be further divided into two sub-layers, which are close to the Cu and the Mg sides, respectively. According to the published results of phase characterization at the joining interface in some other dissimilar FSW joints [15, 20, 30],

the sub-layers can be considered as IMCs layers. Therefore, Fig. 4 illustrates the SEM images with the corresponding EDS point scanning results of various locations at the joining interface with 925 r/min to give a particular investigation of the IMC phases in dissimilar Mg/Cu FSW joints.

As can be seen in the SEM image shown in Fig. 4a, the Mg/Cu joining interface is irregularly distributed from the upper to the lower part of the joint, and the mechanical interlocking can be observed more clearly. Figure 4b–d demonstrates the detailed magnifications of the joining interfaces at the upper, middle and lower parts of the joint, respectively. Figure 4e further shows the EDS point scanning data of the points marked in Fig. 4b–d. In the Mg matrix, a certain number of small Cu pieces with various shapes are peeled off from the Cu matrix because of the intense shear action during tool rotating and finally formed IMC islands after a period of mutual diffusion with the surrounding Mg matrix. In the Cu matrix, some long and lamellar structures are found, which are supposed to be generated by the multiple friction effect between Cu and Mg during the material deposition stage. Similar phenomena in the material matrixes of Al/Cu FSW joint have also been reported [20]. According to the EDS results of points 1, 4, 5, 8, 9 and 12, the IMC of Mg_2Cu and $MgCu_2$ can be identified in the Mg and the Cu matrixes, respectively.

At the Mg/Cu joining interface, the two IMC layers are inferred as layer-A, which consists of $Mg + Mg_2Cu$ next to the Mg matrix, and layer-B, which consists of $MgCu_2 + Mg_2Cu$ next to the Cu matrix, based on the SEM results in Fig. 4 and the Mg-Cu binary phase diagram. As
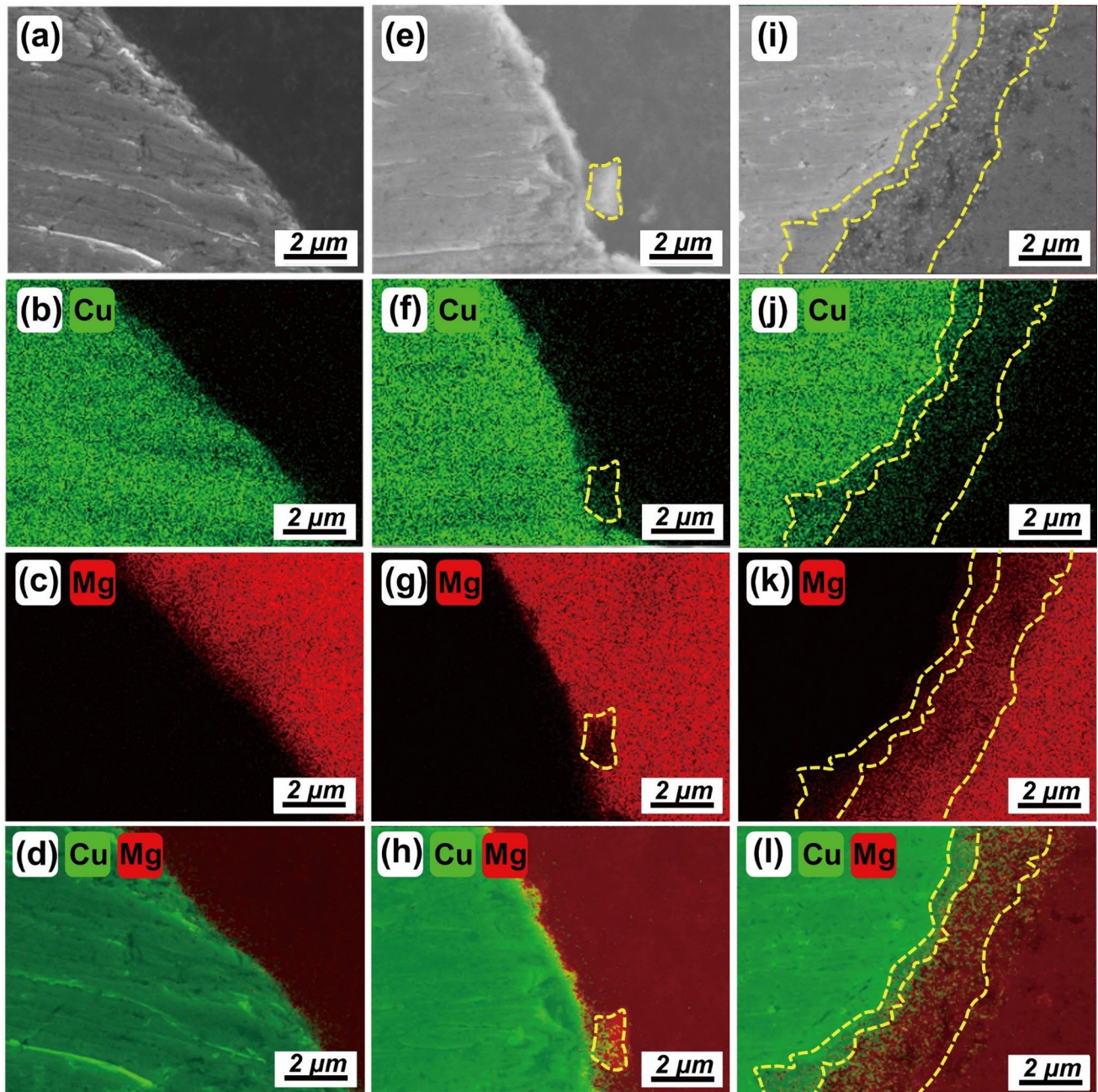
Fig. 3 SEM images **a**, **e** and **i** and corresponding EDS mapping results **b–d**, **f–h**, **j–l** of the bonding interface of welds obtained with three tool rotating speeds: **a–d** 325 r/min, **e–h** 625 r/min, **i–l** 925 r/min

has been widely reported [31–33], the Cu element tends to aggregate with both Mg and Al elements, and the formation of Mg-Cu IMC is much easier than that of Al-Cu IMC due to the limitation of Al element in the matrix of AZ31B alloy. Therefore, the formation of the Mg–Al-Cu ternary phase can be neglected. Moreover, the magnified SEM images give more information about the IMCs of the joining interface at different locations of the Mg/Cu joint. In these figures, the dotted yellow lines depict the boundaries between different

structures. It is shown that the two-layer IMCs are clearly distributed from the upper, middle the lower parts, and their boundaries with Mg or Cu matrix are also distinct.

Figure 4 illustrates that the layer-B ($MgCu_2 + Mg_2Cu$) next to the Cu matrix is much thinner than the layer-A ($Mg + Mg_2Cu$) next to the Mg matrix distributed in the IMCs layer. The thickness of the two IMCs layers at three different locations can be further measured. At the upper region, it can be measured that the total thickness of the Mg/Cu IMCs
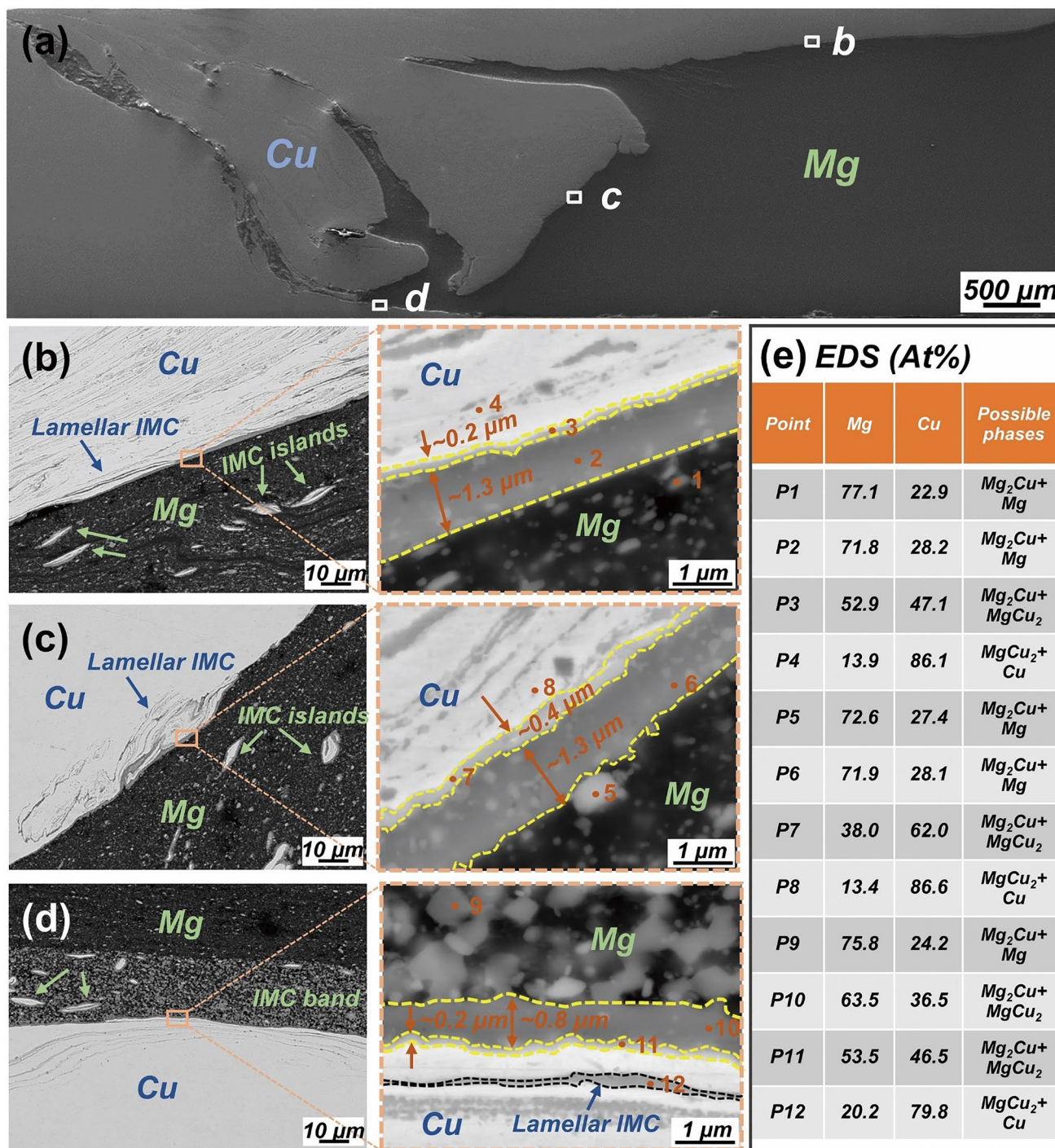
Fig. 4 Microstructures of Mg/Cu FSW joint with 925 r/min: **a** SEM image of the joint, **b–d** magnified SEM images of the joining interface at the upper, middle and lower location of the joint, respectively, **e** EDS point scanning results

layer is approximately 1.5 μm with layer-A and layer-B of 1.3 μm and 0.2 μm, respectively. At the middle region, the values increase to 1.7 μm (1.3 μm for layer-A and 0.4 μm for layer-B). At the lower region, the values decrease to 1.0 μm (0.8 μm for layer-A and 0.2 μm for layer-B). It is shown that the thickness of the IMCs layer first increases, and then

decreases along the Mg/Cu joining interface from the top to the bottom surface at the cross-section of the joints. The same variation tendency of the IMCs thickness has also been reported in FSW joints of other dissimilar materials [30, 34], which is believed to be a result of the thermal and material flow coupled conditions at different weld regions. Moreover,

the average thickness of the Mg/Cu IMCs layer in FSW joint is less than 2.0 μm, which is far thinner than that in the joints by other welding methods [8, 9, 35].

From the X-ray diffraction (XRD) results plotted in Fig. 5, it can be seen that both $MgCu_2$ and Mg_2Cu IMCs did exist in the Mg/Cu FSW joints with various tool rotating speeds. Thus, the primary components of the IMCs in Fig. 4 are verified. The formation and growth of $MgCu_2$ and Mg_2Cu IMCs are controlled by bulk diffusion mechanism during Mg/Cu FSW process. In a bulk diffusion system, the thickness of the IMCs layer, x, follows a parabolic growth law, which is given by [32]:

$$x = k_0 t^{1/2} \cdot \exp\left(-\frac{Q}{RT}\right), \tag{1}$$

where k_0 is the pre-exponential factor, t is the processing time, Q is the activation energy, R is the universal gas constant and T is the temperature. Since the pre-exponential factor k_0 of Mg_2Cu (2.03×10^{-5} m^2/s) is higher than that of $MgCu_2$ (1.45×10^{-5} m^2/s), while the activation energy Q of Mg_2Cu (139.12 kJ/mol) is lower than that of $MgCu_2$ (147.57 kJ/mol) [32], there is no doubt that Mg_2Cu appears preferentially and grows faster than $MgCu_2$ during FSW. As a result, the thickness of Mg_2Cu (layer-A and layer-B) is 4–6 times higher than that of $MgCu_2$ (layer-B). Moreover, with increasing tool rotating speed, both the heat input and the welding temperature are higher, so the thickness of the IMCs layer also increases, as has been shown in Fig. 3. It is also shown that the IMCs layers at the Mg/Cu interface with both 325 r/min and 625 r/min are far too narrow so that different layers can hardly be identified. The formation and

distribution of the IMCs could be another important factor for the mechanical strength of the dissimilar Mg/Cu joint.

3.3 Formation Mechanism of the IMCs

Figure 6 demonstrates a schematic diagram for the formation mechanism of the IMCs during FSW of dissimilar Mg/Cu. With both temperature and strain rate at the interface increasing because of the concurrent friction and shear action by the rotating tool, the diffusions of Cu atoms into Mg matrix and Mg atoms into Cu matrix begin to happen simultaneously. Since the average impurity diffusion coefficients of Mg in Cu were much higher than that of Cu in Mg [32], the diffusion of Mg atom into Cu matrix was faster than that of the Cu atoms in Mg matrix, as schematically shown in Fig. 6a and b. Then, Mg_2Cu is the preferential IMC phase to form at the Mg/Cu interface due to a higher pre-exponential factor and lower activation energy than $MgCu_2$. Therefore, the IMCs layer (layer-A) with Mg_2Cu grows at the Mg side. Since the Mg content in this region is much higher than that in the Mg_2Cu phase, this layer is composed of Mg + Mg_2Cu. Then, more amount of heat is transferred into the Cu side because of the higher thermal conductivity of Cu, which promotes the diffusion of Mg atoms inside the Cu matrix and induces the formation of the $MgCu_2$ IMC phase. As a result, the IMCs layer (layer-B) with $MgCu_2$ + Mg_2Cu forms between the Cu matrix and layer-A. As shown in Fig. 6c, it turns out that layer-B is much thinner than layer-A, and both the two layers with IMCs are composed of two phases, which are Mg + Mg_2Cu for layer-A and $MgCu_2$ + Mg_2Cu for layer-B. Moreover, some more IMCs of Mg_2Cu and $MgCu_2$ also form because of the predominant element contents inside the Mg and Cu matrixes, respectively. In general, the quantity of the Mg_2Cu IMCs is certainly much more than that of the $MgCu_2$ IMCs, as presented in Fig. 6d.

3.4 Mechanical Properties

Figure 7 depicts the micro-hardness distributions on the cross-section of the Mg/Cu FSW joint with various tool rotating speeds. It is shown that the micro-hardness of the Cu and the Mg matrix is about 100 HV$_{0.2}$ and 70 HV$_{0.2}$, respectively. However, the micro-hardness around the pin-affected zone is much higher due to the formation of the IMC phases at the Mg/Cu joining interface. At the tool rotating speed of 925 r/min, the peak value of the micro-hardness reaches 192 HV$_{0.2}$, which is the maximum value among the above parameters. With the tool rotating speed decreasing to 625 r/min and 325 r/min, it has been shown that the total quantity of IMCs decreases dramatically, thus the micro-hardness decreases accordingly.

Figure 8 exhibits the tensile testing results of the Mg/Cu FSW joints with various tool rotating speeds. It can be
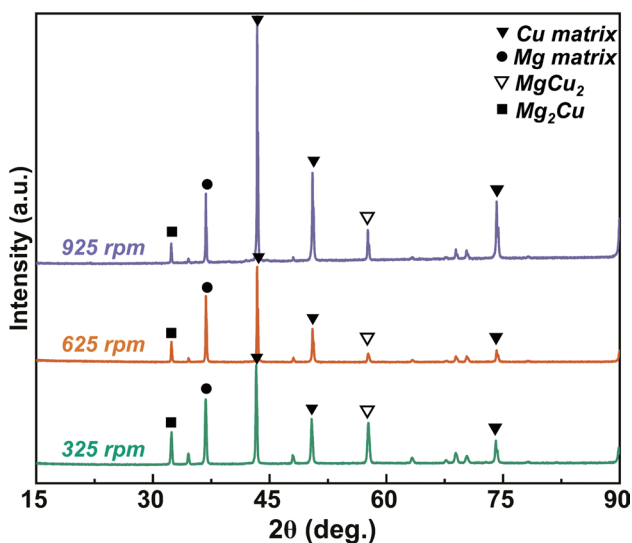

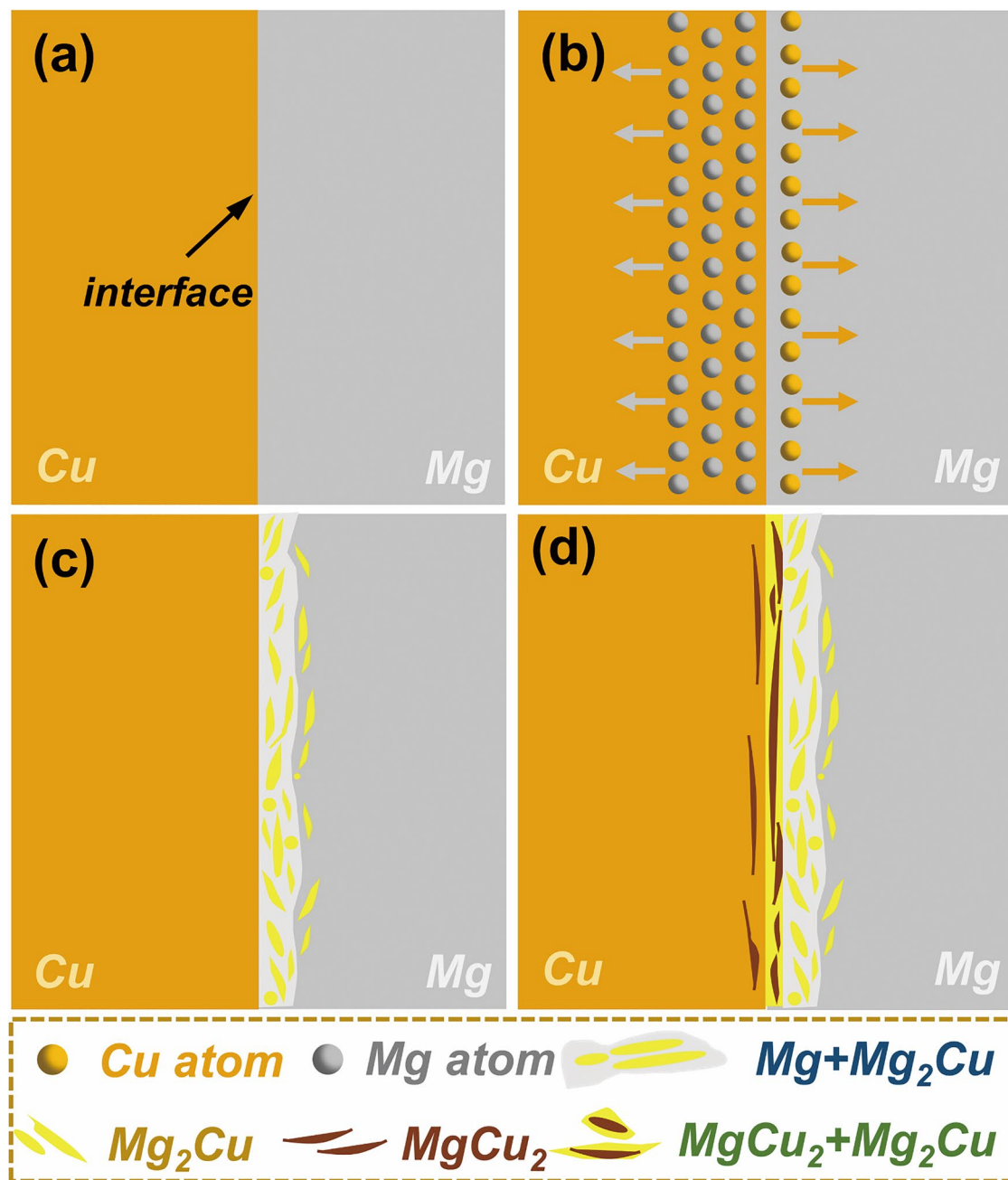**Fig. 5** XRD patterns for the Mg/Cu joints with various tool rotating speeds

Fig. 6 Predicted schematic diagrams of the IMCs formation during Mg/Cu FSW: **a** contact before welding, **b** mutual diffusion of Mg and Cu atoms, **c** formation of IMCs during welding, **d** IMCs formation and distribution results after welding

seen in Fig. 8a that the ultimate tensile strength (UTS) is 114 MPa, 107 MPa and 138 MPa for the joints with 325 r/min, 625 r/min and 925 r/min, respectively. The maximum UTS value is achieved at the highest tool rotating speed of 925 r/min. There are mainly two reasons for this phenomenon. One is that the mechanical interlocking is enhanced with more material flow and intermixing between Mg and Cu. The tortuous fracture interface of the joint at 925 r/min proved the good mixed degree of Mg-Cu materials in the

weld, corresponding to the largest total length of Mg-Cu interface in Fig. 2. The "pinning effect" of a complicated interface is beneficial for hindering the crack propagation [30, 36–38]. The other is that the metallurgical bonding is more sufficient since a clear, uniform and continuous IMCs layer with a thickness between 1.0 μm and 2.0 μm is formed along the Mg/Cu interface, which is believed to be conducive to the improvement of the tensile property of the dissimilar joints [8, 20]. For lower tool rotating speeds,
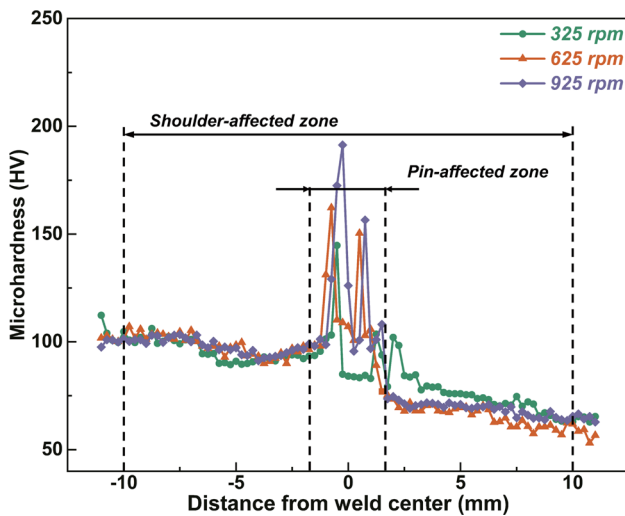
Fig. 7 Micro-hardness distribution on the cross-section of the Mg/Cu FSW joints with various tool rotating speeds

there is no doubt that both the plastic deformation and the heat input are weakened, both the mechanical interlocking and the metallurgical bonding are inadequate, the thickness of IMCs layer is no more than 0.5 μm. It is also shown in Fig. 8a that the fracture locations during the tensile tests are at heat-affected zone of the Cu side for all three tool rotating speeds, which indicates excellent joining at the Mg/Cu interface due to the formation of IMCs layer with proper

thickness. Moreover, the SEM images of the fracture surface for tool rotating speeds of 325 r/min, 625 r/min and 925 r/min are presented in Fig. 8b-d, respectively. Except for the rugged fracture surface, obvious tear ridges and cleavage planes in Fig. 8b-d indicate that brittle fracture is the main fracture mode in the tensile tests of the Mg/Cu FSW joints.

4 Conclusions

1. Defect-free dissimilar Mg/Cu FSW butt joints were obtained with Mg and Cu plates located at the RS and the AS, respectively, at a welding speed of 50 mm/min and tool rotating speeds of 325 r/min, 625 r/min and 925 r/min.
2. Both Mg_2Cu and $MgCu_2$ IMC phases were observed at the Mg/Cu FSW joint. A clear, uniform and continuous IMCs layer was formed at the joining interface, composed of two sub-layers, layer-A of $Mg + Mg_2Cu$ and layer-B of $Mg_2Cu + MgCu_2$.
3. The maximum UTS of the Mg/Cu FSW joint reached 138 MPa at 925 r/min for two main reasons, one was the enhanced mechanical interlocking between Mg and Cu, the other was the sufficient metallurgical bonding at the joining interface with IMCs layer thickness in the range of 1.0–2.0 μm.
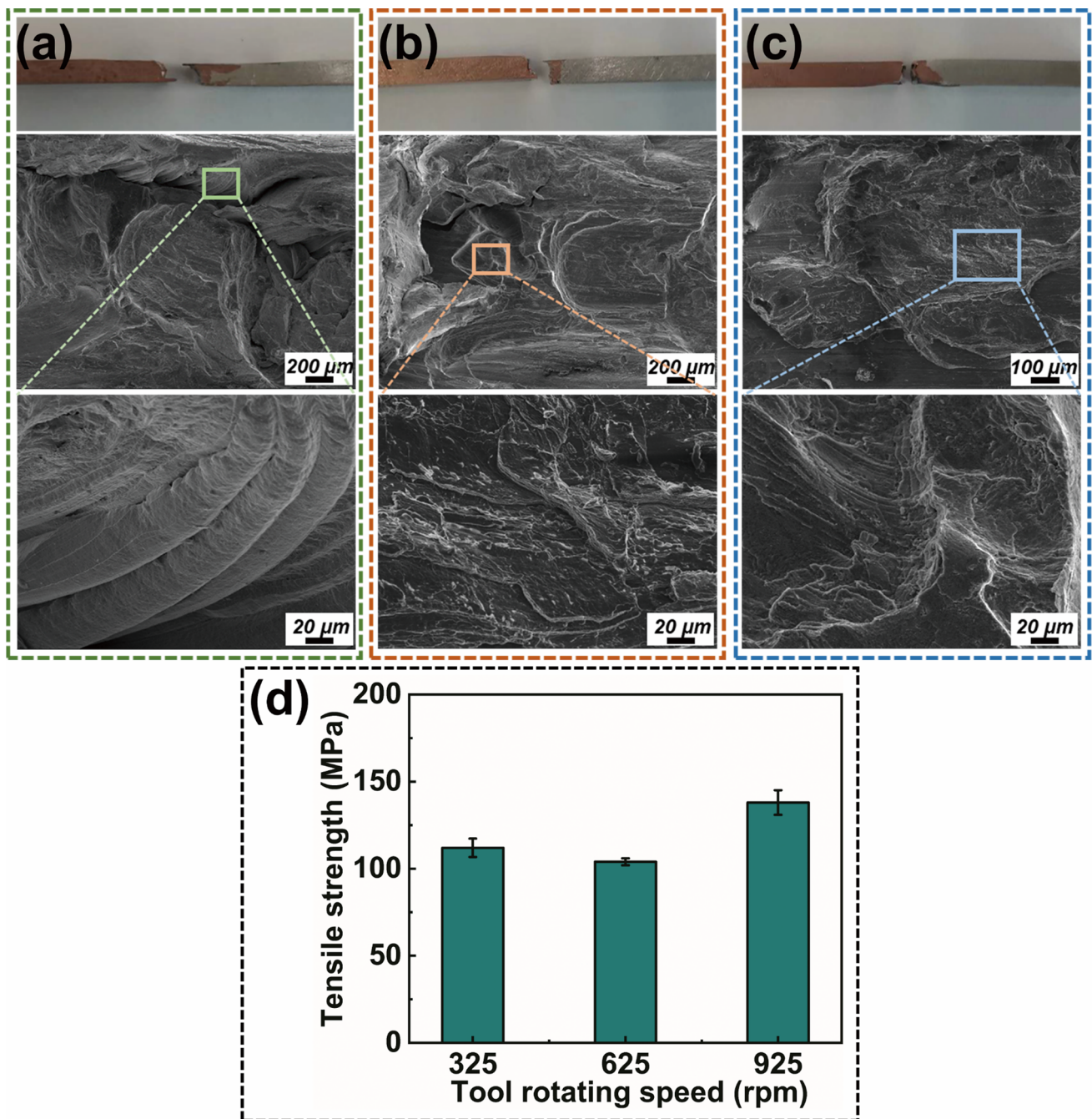
Fig. 8 Tensile testing results of the Mg/Cu FSW joints with various tool rotating speeds, the macroscope of fracture surface and SEM images of fracture locations and magnified fracture surface at **a** 325 r/min, **b** 625 r/min, **c** 925 r/min respectively, **d** the ultimate tensile strength of three tool rating speeds

Declarations

References

[1] J. Zhao, C. Wu, L. Shi, H. Su, J. Mater. Sci. Technol. **139**, 31 (2023)

[2] B.L. Mordike, T. Ebert, Mater. Sci. Eng. A **302**, 37 (2001)

[3] X. Cao, M. Jahazi, J. Immarigeon, W. Wallace, J. Mater. Process. Technol. **171**, 188 (2006)

[4] Z. Sun, J. Ion, J. Mater. Sci. **30**, 4205 (1995)

[5] W. Hou, L.H. Ahmad Shah, G. Huang, Y. Shen, A. Gerlich, J. Alloy. Compd. **825**, 154045 (2020)

[6] P. Alvarez, G. Janeiro, A.A.M. da Silva, E. Aldanondo, A. Echeverria, Sci. Technol. Weld. Join. **15**, 648 (2010)

[7] V.P. Singh, S.K. Patel, N. Kumar, B. Kuriachen, Sci. Technol. Weld. Join. **24**, 653 (2019)

[8] D. Zhao, C. Jiang, K. Zhao, J. Mater. Res. Technol. **23**, 1273 (2023)

[9] H. Shan, Y. Zhang, Y. Li, Z. Luo, J. Manuf. Process. **30**, 570 (2017)

[10] G. Mahendran, V. Balasubramanian, T. Senthilvelan, Trans. Nonferrous Met. Soc. China **20**, 997 (2010)

[11] L. Liu, S. Wang, M. Zhu, Sci. Technol. Weld. Join. **11**, 523 (2006)

[12] P. Venkateswaran, A.P. Reynolds, Mater. Sci. Eng. A **545**, 26 (2012)

[13] M. Kimura, K. Suzuki, M. Kusaka, K. Kaizu, J. Manuf. Process. **26**, 178 (2017)

[14] M. Meisnar, S. Baker, J.M. Bennett, A. Bernad, A. Mostafa, S. Resch, N. Fernandes, A. Norman, Mater. Des. **132**, 188 (2017)

[15] K. Chen, X. Liu, J. Ni, Int. J. Adv. Manuf. Technol. **104**, 1709 (2019)

[16] V. Firouzdor, S. Kou, Metall. Mater. Trans. A **41**, 2914 (2010)

[17] Z.Y. Ma, Metall. Mater. Trans. A **39**, 642 (2008)

[18] R.S. Mishra, Z.Y. Ma, Mater. Sci. Eng. R **50**, 1 (2005)

[19] X. Meng, Y. Huang, J. Cao, J. Shen, J.F. Dos Santos, Prog. Mater. Sci. **115**, 100706 (2021)

[20] P. Xue, B.L. Xiao, D.R. Ni, Z.Y. Ma, Mater. Sci. Eng. A **527**, 5723 (2010)

[21] S. Celik, R. Cakir, Metals **6**, 133 (2016)

[22] J. Zhao, C. Wu, L. Shi, J. Mater. Res. Technol. **17**, 1 (2022)

[23] F. Pan, A. Xu, D. Deng, J. Ye, X. Jiang, A. Tang, Y. Ran, Mater. Des. **110**, 266 (2016)

[24] X. Meng, Y. Xie, S. Sun, X. Ma, L. Wan, J. Cao, Y. Huang, Acta Metall. Sin. -Engl. Lett. **36**, 881 (2023)

[25] S. Ji, X. Cui, L. Ma, H. Liu, Y. Zuo, Z. Zhang, Acta Metall. Sin. -Engl. Lett. **36**, 552 (2023)

[26] S. Nian, M. Li, S. Ji, W. Hu, Z. Zhang, Z. Sun, Chin. J. Aeronaut. **37**, 451 (2024)

[27] Z. Sun, C. Wu, J. Manuf. Process. **36**, 10 (2018)

[28] L.H. Shah, N.H. Othman, A. Gerlich, Sci. Technol. Weld. Join. **23**, 256 (2018)

[29] R. Borrisutthekul, T. Yachi, Y. Miyashita, Y. Mutoh, Mater. Sci. Eng. A **467**, 108 (2007)

[30] J. Zhao, C. Wu, H. Su, J. Manuf. Process. **65**, 328 (2021)

[31] F. Wen, J. Zhao, K. Feng, M. Yuan, D. Zheng, C. Gu, B. Xu, Met. Mater. Int. **28**, 1711 (2022)

[32] J. Dai, B. Jiang, J. Zhang, Q. Yang, Z. Jiang, H. Dong, F. Pan, J. Phase Equilib. Diffus. **36**, 613 (2015)

[33] Y.M. Hwang, P.L. Fan, C.H. Lin, J. Mater. Process. Technol. **210**, 1667 (2010)

[34] H. Su, Q. Zhao, J. Chen, C. Wu, J. Mater. Sci. **57**, 20485 (2022)

[35] A. Macwan, D.L. Chen, Mater. Des. **84**, 261 (2015)

[36] S. Ji, X. Meng, Z. Liu, R. Huang, Z. Li, Mater. Lett. **201**, 173 (2017)

[37] N. Gotawala, A. Shrivastava, CIRP J. Manuf. Sci. Technol. **44**, 70 (2023)

[38] V.P. Singh, D. Kumar, R.P. Mahto, B. Kuriachen, J. Mater. Eng. Perform. **32**, 4185 (2022)